Spin-glass quantum phase transition in amorphous arrays of Rydberg atoms

L. Brodoloni [1,2] J. Vovrosh [3] S. Julià-Farré [3] A. Dauphin [3] and S. Pilati [1,2]

[1] *School of Science and Technology, Physics Division, Università di Camerino, 62032 Camerino, Italy*
[2] *INFN, Sezione di Perugia, I-06123 Perugia, Italy*
[3] *PASQAL SAS, 24 rue Emile Baudot - 91120 Palaiseau, Paris, France*

We perform unbiased quantum Monte Carlo simulations of quantum Ising models defined on amorphous arrays of Rydberg atoms, motivated by a recent proposal for their experimental realization using engineered configurations of the optical tweezers. In contrast to previous studies focusing on periodic geometries, our models are designed to possess well-controlled local structural properties while lacking long-range order. We identify a quantum phase transition from a paramagnetic to a spin-glass phase, characterized via the Edwards-Anderson order parameter computed from the replica overlap. The magnetic structure factor reveals short-range, isotropic antiferromagnetic correlations, and the spin-overlap distribution exhibits a nontrivial form with two broad peaks and significant weight at zero overlap. A comparison with the clean kagome lattice, which shares similar local geometry, underscores the critical role of amorphous structure in stabilizing the spin-glass phase. Our results suggest a promising pathway for the experimental realization of quantum spin glasses using programmable Rydberg atom arrays.

Introduction. Frustrated random interactions in Ising models can give rise to spin-glass phases, which exhibit a variety of intriguing phenomena, including disordered magnetism, memory effects, and possibly the breakdown of ergodicity [1, 2]. In the quantum case, which is the focus of this work, random Ising models are currently being extensively studied to determine whether quantum annealers can achieve a quantum advantage. [3–5]. However, various fundamental questions are still unanswered, e.g., if and where replica symmetry breaking (RSB) occurs [6–12], whether the spin-glass transition survives longitudinal fields [13–16], or how the spin-glass transition relates to the many-body localization transition [17–20].

Today, many outstanding open theoretical questions are being addressed by performing quantum simulations on various experimental platforms. In fact, paradigmatic quantum Ising Hamiltonians have been implemented using ultracold atomic gases [21, 22], trapped ions [23], superconducting qubits [24], or neutral atoms precisely positioned using optical tweezers and then coupled to the Rydberg state [25–27]. For the latter platform, previous theoretical studies focused mainly on periodic arrangements of the tweezers, including one-dimensional and two-dimensional (2D) configurations, such as square, triangular, and kagome periodic lattices [28–35]. Depending on the specific periodic geometry, different magnetically ordered phases have been predicted and in some cases already been experimentally observed [36–38]. Incommensurate phases that separate magnetically ordered and paramagnetic phases have also been studied in single-leg and double-leg chains [39–43]. However, quantum spin-glass phases have not been discussed yet. Memory effects associated with glassy behavior were observed in computer simulations at the boundary of differently ordered phases [44], but this finding has been questioned [45].

In general, frustration effects may be induced by the lattice geometry and/or by random ferromagnetic and antiferromagnetic interactions. In Rydberg-atom platforms, the interatomic couplings are always antiferromagnetic. On the other hand, the atomic layout is essentially arbitrary [46–48], which in turn allows some randomization of the couplings, since these depend on the interatomic distances [49]. This flexibility has been exploited to address combinatorial optimization problems [46, 50, 51], machine-learning tasks [52–54], and topological phases [55, 56]. As recently shown [57], amorphous solids can also be realized, namely, configurations exhibiting well-defined short-range structural order in the absence of long-range positional or orientational order. However, the phase diagram of quantum Ising models with positionally disordered couplings remains largely unexplored, and it is unclear whether antiferromagnetic couplings alone are sufficient to induce spin-glass phases.

In this paper, we employ unbiased quantum Monte Carlo (QMC) simulations to investigate the ground-state properties of quantum Ising models defined on amorphous arrays. On the one hand, the coordination number and the preferred bond angles are set to mimic those of the periodic kagome lattice, as shown in Fig. 1. On the other hand, the interactions are antiferromagnetic and decay with the sixth power of the distance, as in Rydberg-atom experiments. This setup is intended to combine the frustration effects occurring in the kagome lattice with positional disorder of the couplings. We determine the static magnetic structure factor and the replica-overlap Edwards-Anderson (EA) order parameter. The latter is suitable for identifying spin-glass phases, and we indeed find clear indications of a quantum phase transition from a paramagnetic to a spin-glass phase. The critical transverse field is determined via a finite-size scaling analysis. The magnetic structure factor indicates that, in the spin-glass regime, the antiferromagnetic correlations are short-ranged and isotropic, denoting the absence of spatial ordering. We also analyze the spin-overlap distribution for the feasible sizes. To highlight the role of the amorphous structure, we make a comparison with results corresponding to the periodic kagome lattice.

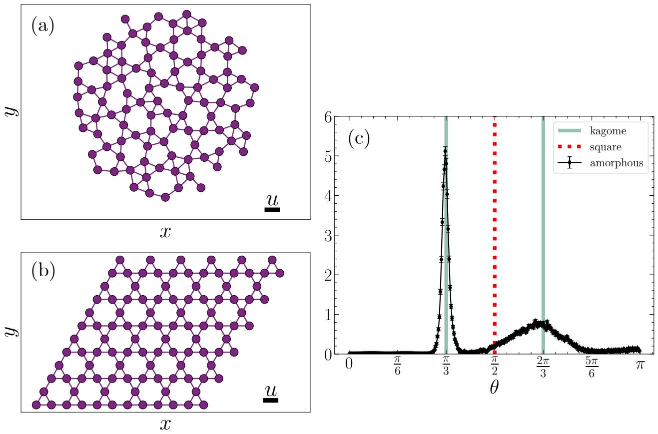

FIG. 1. Panels (a) and (b): representation of a 2D amorphous array (a) and of the kagome lattice (b). Segments connect nearest-neighbor atoms. Panel (c): probability distribution of bond-angle θ in the amorphous arrays. The vertical lines denote the angles of the kagome lattice (continuous lines) and of the square lattice (dashed line), with periodic boundary conditions.

Models and methods. We simulate a 2D transverse field Ising Hamiltonian, which reads

$$H = \sum_{i<j} J_{ij}\sigma_i^z\sigma_j^z - \Gamma\sum_{i=1}^{N}\sigma_i^x. \tag{1}$$

Here, σ_i^α, for $\alpha = x, z$, are usual Pauli operators acting on the spin $i = 1, \ldots, N$ at position $\mathbf{r}_i$. Γ is the uniform transverse magnetic field, and the couplings J_{ij} follow a power-low decay with respect to the distance: $J_{ij} = J_0/|\mathbf{r}_i - \mathbf{r}_j|^6$. J_0 is set as the energy unit. These parameters describe the Ising model that can be implemented in neutral atom quantum simulators. Notice that, to fulfill the Z_2 symmetry of the above Hamiltonian, local addressing of the detuning is required to compensate longitudinal terms [58, 59]. Although not trivial, considering the most recent experimental developments, this compensation is feasible [60–62].

The amorphous configurations $(\mathbf{r}_1, \ldots, \mathbf{r}_N)$ are created starting from the algorithm described in Ref. [57]. An exemplary array is visualized in Fig. 1, panel (a). In short, the algorithm allows us to control the coordination number C, defined as the average number of atoms closer than the first minimum of the pair correlation function. Here, we set $C \approx 4$, which corresponds to either (clean) kagome or square lattices. In fact, an appropriate choice of the kernel function favors the former. More details are provided in the Supplemental Material [63]. Indeed, the bond-angle distribution displays sizable broad peaks at the angles corresponding to the kagome lattice, namely $\theta = \pi/3$ and $\theta = 2\pi/3$, and essentially no weight at the angle $\theta = \pi/2$ occurring in the square lattice (see panel (c) of Fig 1). The average nearest-neighbor distance is $1.062(2)u$, where u is the length unit shown in Fig. 1. To favor future studies, the amorphous arrays employed in this Article are provided via the public repository at Ref. [64]. To highlight the role of the lack of long-range structural order, below we also discuss the QMC results for the clean kagome lattice with periodic boundary conditions and nearest-neighbor distance u.

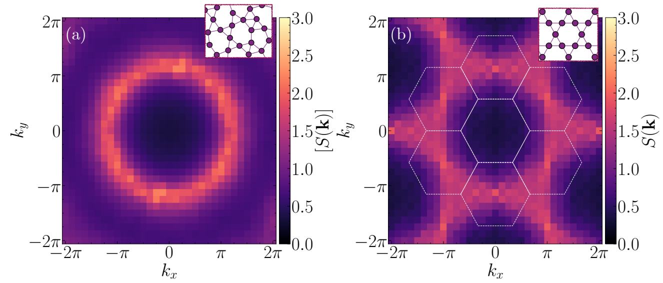

FIG. 2. Panels (a) and (b): magnetic structure factor $S(\mathbf{k})$ versus k_x and k_y, with $\mathbf{k} = (k_x, k_y)$, for (ensemble-averaged) amorphous arrays (a) and for the periodic kagome lattice (b). In panel (b), the (white) hexagons represent the Brillouin zones.

The ground state of the Hamiltonian (1) is simulated using the continuous-time projection QMC algorithm detailed in Refs. [65–67]. It is verified that the possible systematic bias due to the population control [68–70] is below statistical uncertainties and the pure estimators are obtained via the standard forward-walking technique [71]. The guiding wave function is a neural network state in the form of a restricted Boltzmann machine [72], which is trained using the self-learning protocol of Ref. [73]. A relevant benefit of this QMC method is the absence of imaginary time discretization errors. On the other hand, finite-temperature path-integral Monte Carlo simulations with discrete imaginary time would probably allow reaching larger sizes than those considered below [74–76]. However, these simulations are performed at a finite temperature and thus need a two-parameter scaling ansatz or a rescaling criterion in the analysis of zero-temperature phase transitions via finite-size scaling. In general, QMC algorithms allow simulating power-law interactions without the truncations usually implemented in relevant alternative computational methods based on tensor-network methods [77]. A viable QMC algorithm might also be the stochastic series expansion method [78, 79]. For the amorphous arrays, open boundary simulations are performed, while for the kagome lattice we implement periodic boundary conditions and account also for the first periodic images beyond the fundamental simulation cell, given that the couplings with further-apart images are negligible.

Magnetic structure factor. The first observable we analyze is the static magnetic structure factor, defined as $S(\mathbf{k}) = \langle \mathcal{S}^z(\mathbf{k})\mathcal{S}^z(-\mathbf{k})\rangle$, where $\mathcal{S}^z(\mathbf{k}) = N^{-1/2}\sum_i \sigma_i^z \exp(i\mathbf{k}\cdot\mathbf{r}_i)$, which is suitable to identify (possibly long range) magnetic correlations both in periodic and nonperiodic systems. For the amorphous arrays, the ensemble-average – denoted with $[S(\mathbf{k})]$ – is determined considering $N_r = 30$ realizations. The re-

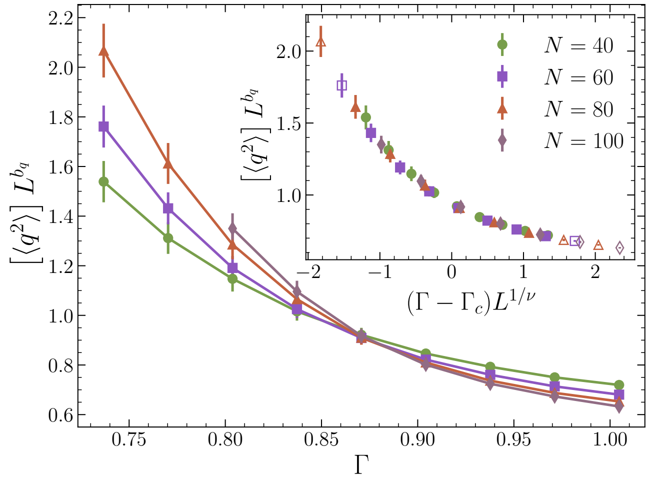

FIG. 3. Main panel: rescaled (disordered averaged) EA order parameter $[\langle q^2\rangle] L^{b_q}$ as a function of the transverse field Γ. Different datasets correspond to different system sizes. Inset: universal collapse of $[\langle q^2\rangle] L^{b_q}$ plotted as a function of the transverse field $(\Gamma - \Gamma_c) L^{1/\nu}$. The critical parameters Γ_c, $1/\nu$, and b_q are obtained by optimizing the data collapse [80], excluding the data shown as empty symbols.

Couplings	$1/\nu$	b_q	Γ_c	Ref.
50% ±1	1.02(16)	1.76(3)	2.11(1)	[76]
50% ±1	0.71(24)(9)	1.73(8)(8)	2.18(1)	[74]
$\mathcal{N}(0,1)$	1.11(22)	1.68(8)	1.98(7)	[84]
$\propto 1/r^6$	1.22(45)	1.63(12)	0.864(33)	This work

TABLE I. Critical exponents ν and b_q and transition point Γ_c for different choices of random couplings J_{ij}, namely, binary random values (50% ±1) and Gaussian values $\mathcal{N}(0,1)$ on the square lattice, and the positional disorder decaying as $\propto 1/r^6$ considered in this Article. Numbers in parentheses denote the errorbar. Where two numbers are given, the first denotes the statistical uncertainty, the second the systematic effects.

sults at transverse field $\Gamma = 0.737$ display a broad circular hill, corresponding to isotropic magnetic correlations (see Fig. 2). The peak height does not scale with the system size (see Supplemental Material [63]), meaning that these correlations decay with distance. In the periodic kagome lattice, we again find a broad continuum, but this follows the hexagonal structure of the Brillouin zones. Notice that also in this case the correlations have a short-range character, pointing to a paramagnetic ground state, as found in previous studies addressing kagome Ising models with nearest-neighbor antiferromagnetic interactions [81, 82]. As discussed below, the system with $\Gamma = 0.737$ is in the spin-glass regime.

Replica-overlap Edwards-Anderson order parameter. To identify the spin-glass phase, we analyze the (mean squared) EA order parameter $\langle \hat{q}^2\rangle$, which can be evaluated without systematic bias considering the overlap operator $\hat{q}$ between two identical replicas of the system [83]; $\hat{q}$ is defined as

$$\hat{q} = \frac{1}{N}\sum_{i=1}^{N} \sigma^z_{a,i}\sigma^z_{b,i}. \tag{2}$$

Here, the subscripts a and b denote the two replicas, which are simulated within the projection QMC algorithm by evolving a two-fold replicated Hamiltonian $H_T = H_a + H_b$ [84], where $H_{a/b}$ are defined as in Eq. (1) with Pauli matrices $\sigma^\alpha_{a/b,i}$. The ensemble average $[\langle \hat{q}^2\rangle]$ is performed over $N_r \in [100 : 200]$ amorphous arrays. Close to the critical point Γ_c, one assumes the following scaling Ansatz with a critical exponent b_q [76]: $[\langle \hat{q}^2\rangle] L^{b_q} = f(x)$, where $f(x)$ is a universal function of the reduced transverse field $x = (\Gamma - \Gamma_c)L^{1/\nu}$ and ν is the correlation-length critical exponent. The linear size is defined as $L = \sqrt{N}$. The critical parameters are obtained by optimizing the data collapse using the software available from Refs. [80, 85], which minimizes deviations from a self-consistently derived master curve [86]. Restricting the scaling analysis to $|x| \leq 1.34$, we obtain the following estimates: $\Gamma_c = 0.864(33)$, $b_q = 1.63(12)$, and $1/\nu = 1.22(45)$. Smaller fitting windows provide comparable estimates. We empirically observe that the universal critical parameters b_q and ν turn out to be consistent with recent estimates for the 2D quantum EA Hamiltonian on the square lattice with binary or Gaussian random couplings [74, 76, 84], within the statistical errorbars. The comparison is detailed in Table I. This consistency might be attributed to the short-range character of the r^{-6} power-law interaction and the presence of only short-range statistical correlations in the positionally randomized couplings, possibly leading to the same universality class of the 2D quantum EA model. Taking into account the relatively large uncertainty, our estimate of $1/\nu$ is also consistent with the bound $1/\nu \leq D/2$ [87]. Note that, due to finite-size corrections to the universal scaling ansatz, this estimate was found to slightly decrease when the smallest system sizes were not included in the scaling analysis [74]. This effect cannot be discerned here because of the large statistical uncertainty and the limited largest sizes. In fact, large-scale QMC simulations performed well within the spin-glass phase are computationally demanding due to the slow stochastic dynamics. On the other hand, the comparison of the parameter b_q with previous results from the literature is more stringent. As already noted [74], the values obtained for b_q denote a very slow divergence of the spin-glass susceptibility $\chi_{\mathrm{SG}} = [\langle \hat{q}^2\rangle] L^2$ at the critical point.

Replica overlap distribution. To shed some light on the nature of the spin-glass phase of the amorphous arrays, we analyze the distribution of the ensemble-averaged replica spin-overlap $P(q) = [P_J(q)]$ at $\Gamma = 0.67$; for a single realization, this distribution is computed as: $P_J(q) = \langle \delta(q - \hat{q})\rangle$. Simulations of $P(q)$ are often used to assess the applicability of any of the most prominent theories of the spin-glass phase, in particular the droplet-

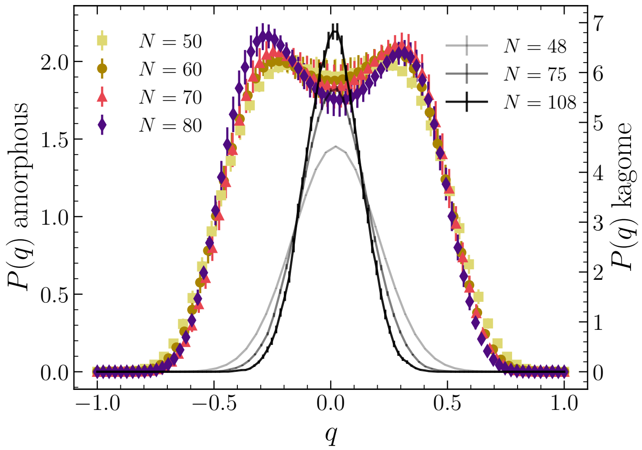

FIG. 4. Distribution of the replica spin-overlap distribution $P(q)$ for the (ensemble averaged) amorphous arrays (left vertical axis) and for the kagome lattice (right vertical axis). Different datasets correspond to different sizes L. The transverse field is $\Gamma = 0.67 < \Gamma_c$.

picture or the RSB scenario [88, 89]. While the first theory predicts two δ-function peaks in the thermodynamic limit, the latter predicts a nontrivial distribution with a sizable weight at $q = 0$. Our QMC results at $\Gamma = 0.67$ are shown in Fig. 4. For the feasible sizes, we find a distribution with two (symmetry related) broad peaks and sizable values of $P(q = 0)$. Yet, approaching the thermodynamic limit $L \to \infty$ is notoriously problematic and, given the limited system sizes we address, it is not possible to perform a reliable extrapolation [90–92]. Furthermore, while for the smaller sizes essentially all realizations satisfy the expected symmetry $P_J(q) = P_J(-q)$, with the largest size $L = 80$ some realizations break the symmetry for the feasible simulation time, leading to a small asymmetry of $P(q)$. It is worth comparing the replica overlap distribution of amorphous arrays with the one corresponding to the periodic kagome lattice at the same transverse field. In the latter case, we find a narrow single-peak distribution that shrinks in the thermodynamic limit. Furthermore, the spin-glass susceptibility does not increase with system size, at least in the range $\Gamma \in [0.67, 1.34]$ [63]. This highlights the important role of the absence of long-range structural order of the optical tweezers, compared to a periodic lattice with similar local structural properties.

Summary. We have investigated the ground-state properties of quantum Ising models with positional disorder using unbiased neural QMC simulations. The Hamiltonian was designed to describe Rydberg atoms arranged in 2D amorphous arrays, whose local structural properties mimic those of kagome lattices. Notably, the finite-size scaling analysis of the EA order parameter revealed the occurrence of a quantum phase transition from a paramagnetic to a spin-glass phase. The critical exponents turned out to be consistent, within the statistical uncertainties, with those corresponding to the 2D EA model with transverse field. By contrast, the results corresponding to the periodic kagome lattice display no hint of glassy behavior. This highlights the important role of the aperiodic structure of the amorphous arrays and suggests that frustration effects in clean periodic systems are not sufficient to induce a spin-glass phase. Both the amorphous and the kagome setups host short-range antiferromagnetic correlations. However, these are isotropic in the former case, whereas they display a six-fold orientational symmetry in the latter. Notably, the ground state of the kagome lattice is paramagnetic in the explored parameter regime.

Outlook. Our results indicate that positionally distorted antiferromagnetic interactions can give rise to a spin-glass quantum phase transition. This finding opens a promising pathway to experimentally observe this phenomenon in Rydberg-atom platforms, which would allow addressing outstanding open problems on the nature of the spin-glass phase via quantum simulations. As next steps, it would be interesting to explore if and how spin-glass behavior occurs in Hamiltonians without local detuning compensations and how the spin-glass phase could be prepared using quantum annealing protocols. The former issue is related to the possible existence of the quantum Almeida-Thouless line [13, 14], i.e, to whether RSB occurs also in the presence of longitudinal fields, or whether, instead, a paramagnetic or a replica-symmetric spin-glass phase forms. The most recent studies on the quantum Sherrington-Kirkpatrick model found that RSB occurs also at finite longitudinal fields [13, 93], although the spin-glass transition might be broadened [16]. Little is known about finite-dimensional lattices –let alone realistic Rydberg Hamiltonians – and addressing this issue lies beyond the scope of this initial study. Temperature effects are also worth studying. It is known that, in the case of power-law decaying random interactions on periodic lattices, the classical spin-glass phase transition might occur at finite or zero temperature depending on the power [94–96]; on the other hand, the case of finite-temperature amorphous arrays has not been studied. Anyway, the 2D quantum phase transition has strong effects in the critical dynamics [76], meaning that spin-glass phenomena are anyway expected also at finite temperature. The possible connection between the spin-glass and the many-body localization transitions is also worth investigating [97–99], and this would probably require entering the small transverse field regime. The spin-glass phase could also be characterized using entanglement measures [100–102]. Paradigmatic spin-glass models can also be implemented in quantum annealers built with superconducting-flux qubits [76], but these devices do not allow readout at finite transverse fields, except indirectly via anneal-pause protocols [82]. Trapped ions are promising alternative platforms. Many-body localization has already been observed in a chain of ten ions [103]. Yet, ion traps are still limited to one-dimensional geometries and fewer spins, although small 2D crystals have recently been implemented [104]. On the other hand, 2D arrays of several thousands of neutral atoms have already been realized [105, 106]. Future studies could address other types of positional disorder, other forms of correlated aperiodic couplings, e.g., quasi-crystals featuring long-range orientational order, randomly distorted frustrated lattices, or longer-range interactions relevant for trapped ions [107].

ACKNOWLEDGMENTS

Acknowledgments— We thank L. Fallani, L. Guariento, V. Gavryusev, V. Vitale, T. M. Santos, I. González-Adalid Pemartín and V. Martín-Mayor, for useful discussions. Support from the following sources is acknowledged: PNRR MUR project PE0000023-NQSTI; PRIN 2022 MUR project "Hybrid algorithms for quantum simulators" – 2022H77XB7; PRIN-PNRR 2022 MUR project "UEFA" – P2022NMBAJ; National Centre for HPC, Big Data and Quantum Computing (ICSC), CN00000013 Spoke 7 – Materials & Molecular Sciences; CINECA awards ISCRA IsCc2_REASON, INF24_lincoln, and INF24_lincoln; EuroHPC Joint Undertaking for awarding access to the EuroHPC supercomputer LUMI, hosted by CSC (Finland), through EuroHPC Development and Regular Access calls. Pasqal's team acknowledges funding from the European Union the projects EQUALITY (Grant Agreement 101080142) and PASQuanS2.1 (HORIZON-CL4-2022-QUANTUM02-SGA, Grant Agreement 101113690)

Data availability: To favor future numerical and experimental investigations, the coordinates of the amorphous configurations employed in this Article are made available at the repository in Ref. [64]. All other data are available from the corresponding author upon reasonable request.

[1] K. Binder and A. P. Young, Spin glasses: Experimental facts, theoretical concepts, and open questions, Rev. Mod. Phys. **58**, 801 (1986).
[2] P. Charbonneau, E. Marinari, G. Parisi, F. Ricci-tersenghi, G. Sicuro, F. Zamponi, and M. Mezard, *Spin Glass Theory and Far Beyond: Replica Symmetry Breaking after 40 Years* (World Scientific, 2023).
[3] G. E. Santoro, R. Martoňák, E. Tosatti, and R. Car, Theory of quantum annealing of an Ising spin glass, Science **295**, 2427 (2002).
[4] S. Tanaka, R. Tamura, and B. K. Chakrabarti, *Quantum spin glasses, annealing and computation* (Cambridge University Press, 2017).
[5] P. Hauke, H. G. Katzgraber, W. Lechner, H. Nishimori, and W. D. Oliver, Perspectives of quantum annealing: methods and implementations, Rep. Prog. Phys. **83**, 054401 (2020).
[6] Y. Y. Goldschmidt, Solvable model of the quantum spin glass in a transverse field, Phys. Rev. B **41**, 4858 (1990).
[7] G. Büttner and K. D. Usadel, Stability analysis of an Ising spin glass with transverse field, Phys. Rev. B **41**, 428 (1990).
[8] D. Thirumalai, Q. Li, and T. R. Kirkpatrick, Infinite-range Ising spin glass in a transverse field, J. Phys. A **22**, 3339 (1989).
[9] N. Read, S. Sachdev, and J. Ye, Landau theory of quantum spin glasses of rotors and Ising spins, Phys. Rev. B **52**, 384 (1995).
[10] P. Ray, B. K. Chakrabarti, and A. Chakrabarti, Sherrington-kirkpatrick model in a transverse field: Absence of replica symmetry breaking due to quantum fluctuations, Phys. Rev. B **39**, 11828 (1989).
[11] S. Mukherjee, A. Rajak, and B. K. Chakrabarti, Classical-to-quantum crossover in the critical behavior of the transverse-field Sherrington-Kirkpatrick spin glass model, Phys. Rev. E **92**, 042107 (2015).
[12] H. Leschke, C. Manai, R. Ruder, and S. Warzel, Existence of replica-symmetry breaking in quantum glasses, Phys. Rev. Lett. **127**, 207204 (2021).
[13] A. P. Young, Stability of the quantum Sherrington-Kirkpatrick spin glass model, Phys. Rev. E **96**, 032112 (2017).
[14] C. Manai and S. Warzel, The de Almeida–Thouless line in hierarchical quantum spin glasses, Journal of Statistical Physics **186**, 14 (2022).
[15] A. Kiss, G. Zaránd, and I. Lovas, Complete replica solution for the transverse field Sherrington-Kirkpatrick spin glass model with continuous-time quantum Monte Carlo method, Phys. Rev. B **109**, 024431 (2024).
[16] P. M. Schindler, T. Guaita, T. Shi, E. Demler, and J. I. Cirac, Variational ansatz for the ground state of the quantum Sherrington-Kirkpatrick model, Phys. Rev. Lett. **129**, 220401 (2022).
[17] C. R. Laumann, A. Pal, and A. Scardicchio, Many-body mobility edge in a mean-field quantum spin glass, Phys. Rev. Lett. **113**, 200405 (2014).
[18] J. A. Kjäll, J. H. Bardarson, and F. Pollmann, Many-body localization in a disordered quantum Ising chain, Phys. Rev. Lett. **113**, 107204 (2014).
[19] G. Mossi, T. Parolini, S. Pilati, and A. Scardicchio, On the quantum spin glass transition on the Bethe lattice, J. Stat. Mech.: Theory Exp. **2017** (1), 013102.
[20] L. Rademaker and D. A. Abanin, Slow nonthermalizing dynamics in a quantum spin glass, Phys. Rev. Lett. **125**, 260405 (2020).
[21] I. Bloch, J. Dalibard, and S. Nascimbene, Quantum simulations with ultracold quantum gases, Nat. Phys. **8**, 267 (2012).
[22] M. Lewenstein, A. Sanpera, and V. Ahufinger, *Ultracold Atoms in Optical Lattices: Simulating quantum many-body systems* (Oxford University Press, Oxford (UK), 2012).
[23] R. Blatt and C. F. Roos, Quantum simulations with trapped ions, Nat. Phys. **8**, 277 (2012).
[24] A. A. Houck, H. E. Türeci, and J. Koch, On-chip quantum simulation with superconducting circuits, Nat. Phys. **8**, 292 (2012).
[25] P. Schauss, Quantum simulation of transverse Ising models with Rydberg atoms, Quantum Sci. Technol. **3**, 023001 (2018).

[26] A. Browaeys and T. Lahaye, Many-body physics with individually controlled Rydberg atoms, Nature Physics **16**, 132 (2020).

[27] L. Henriet, L. Beguin, A. Signoles, T. Lahaye, A. Browaeys, G.-O. Reymond, and C. Jurczak, Quantum computing with neutral atoms, Quantum **4**, 327 (2020).

[28] S. Humeniuk, Quantum monte carlo study of long-range transverse-field Ising models on the triangular lattice, Phys. Rev. B **93**, 104412 (2016).

[29] R. Samajdar, W. W. Ho, H. Pichler, M. D. Lukin, and S. Sachdev, Complex density wave orders and quantum phase transitions in a model of square-lattice Rydberg atom arrays, Phys. Rev. Lett. **124**, 103601 (2020).

[30] M. Kalinowski, R. Samajdar, R. G. Melko, M. D. Lukin, S. Sachdev, and S. Choi, Bulk and boundary quantum phase transitions in a square Rydberg atom array, Phys. Rev. B **105**, 174417 (2022).

[31] M. J. O'Rourke and G. K.-L. Chan, Entanglement in the quantum phases of an unfrustrated Rydberg atom array, Nat. Commun. **14**, 5397 (2023).

[32] S. Guo, J. Huang, J. Hu, and Z.-X. Li, Order by disorder and an emergent Kosterlitz-Thouless phase in a triangular Rydberg array, Phys. Rev. A **108**, 053314 (2023).

[33] S. Yang and J.-B. Xu, Density-wave-ordered phases of Rydberg atoms on a honeycomb lattice, Phys. Rev. E **106**, 034121 (2022).

[34] M. Sarkar, M. Pal, A. Sen, and K. Sengupta, Quantum order-by-disorder induced phase transition in Rydberg ladders with staggered detuning, SciPost Phys. **14**, 004 (2023).

[35] R. Samajdar, W. W. Ho, H. Pichler, M. D. Lukin, and S. Sachdev, Quantum phases of Rydberg atoms on a kagome lattice, Proc. Natl. Acad. Sci. U.S.A. **118**, e2015785118 (2021).

[36] P. Scholl, M. Schuler, H. J. Williams, A. A. Eberharter, D. Barredo, K.-N. Schymik, V. Lienhard, L.-P. Henry, T. C. Lang, T. Lahaye, *et al.*, Quantum simulation of 2D antiferromagnets with hundreds of Rydberg atoms, Nature **595**, 233 (2021).

[37] S. Ebadi, T. T. Wang, H. Levine, A. Keesling, G. Semeghini, A. Omran, D. Bluvstein, R. Samajdar, H. Pichler, W. W. Ho, *et al.*, Quantum phases of matter on a 256-atom programmable quantum simulator, Nature **595**, 227 (2021).

[38] C. Chen, G. Bornet, M. Bintz, G. Emperauger, L. Leclerc, V. S. Liu, P. Scholl, D. Barredo, J. Hauschild, S. Chatterjee, *et al.*, Continuous symmetry breaking in a two-dimensional Rydberg array, Nature **616**, 691 (2023).

[39] H. Weimer and H. P. Büchler, Two-stage melting in systems of strongly interacting Rydberg atoms, Phys. Rev. Lett. **105**, 230403 (2010).

[40] M. Rader and A. M. Läuchli, Floating phases in one-dimensional Rydberg ising chains, arXiv:1908.02068 https://doi.org/10.48550/arXiv.1908.02068 (2019).

[41] X.-J. Yu, S. Yang, J.-B. Xu, and L. Xu, Fidelity susceptibility as a diagnostic of the commensurate-incommensurate transition: A revisit of the programmable rydberg chain, Phys. Rev. B **106**, 165124 (2022).

[42] J. Soto-Garcia and N. Chepiga, Numerical investigation of quantum phases and phase transitions in a two-leg ladder of Rydberg atoms, Phys. Rev. Res. **7**, 013215 (2025).

[43] J. Zhang, S. H. Cantú, F. Liu, A. Bylinskii, B. Braverman, F. Huber, J. Amato-Grill, A. Lukin, N. Gemelke, A. Keesling, *et al.*, Probing quantum floating phases in Rydberg atom arrays, Nat. Commun. **16**, 712 (2025).

[44] Z. Yan, Y.-C. Wang, R. Samajdar, S. Sachdev, and Z. Y. Meng, Emergent glassy behavior in a kagome Rydberg atom array, Phys. Rev. Lett. **130**, 206501 (2023).

[45] M. Hibat-Allah, E. Merali, G. Torlai, R. G. Melko, and J. Carrasquilla, Recurrent neural network wave functions for Rydberg atom arrays on kagome lattice, arXiv:2405.20384 https://doi.org/10.48550/arXiv.2405.20384 (2024).

[46] S. Ebadi, A. Keesling, M. Cain, T. T. Wang, H. Levine, D. Bluvstein, G. Semeghini, A. Omran, J.-G. Liu, R. Samajdar, X.-Z. Luo, B. Nash, X. Gao, B. Barak, E. Farhi, S. Sachdev, N. Gemelke, L. Zhou, S. Choi, H. Pichler, S.-T. Wang, M. Greiner, V. Vuletić, and M. D. Lukin, Quantum optimization of maximum independent set using Rydberg atom arrays, Science **376**, 1209 (2022), https://www.science.org/doi/pdf/10.1126/science.abo6587.

[47] M.-T. Nguyen, J.-G. Liu, J. Wurtz, M. D. Lukin, S.-T. Wang, and H. Pichler, Quantum optimization with arbitrary connectivity using Rydberg atom arrays, PRX Quantum **4**, 010316 (2023).

[48] M. Kim, K. Kim, J. Hwang, E.-G. Moon, and J. Ahn, Rydberg quantum wires for maximum independent set problems, Nature Physics **18**, 755 (2022).

[49] R. Menu and T. Roscilde, Anomalous diffusion and localization in a positionally disordered quantum spin array, Phys. Rev. Lett. **124**, 130604 (2020).

[50] L. Leclerc, C. Dalyac, P. Bendotti, R. Griset, J. Mikael, and L. Henriet, Implementing transferable annealing protocols for combinatorial optimization on neutral-atom quantum processors: A case study on smart charging of electric vehicles, Phys. Rev. A **111**, 032611 (2025).

[51] P. Cazals, A. François, L. Henriet, L. Leclerc, M. Marin, Y. Naghmouchi, W. da Silva Coelho, F. Sikora, V. Vitale, R. Watrigant, M. W. Garzillo, and C. Dalyac, Identifying hard native instances for the maximum independent set problem on neutral atoms quantum processors, arXiv:2502.04291 https://doi.org/10.48550/arXiv.2502.04291 (2025).

[52] B. Albrecht, C. Dalyac, L. Leclerc, L. Ortiz-Gutiérrez, S. Thabet, M. D'Arcangelo, J. R. K. Cline, V. E. Elfving, L. Lassablière, H. Silvério, B. Ximenez, L.-P. Henry, A. Signoles, and L. Henriet, Quantum feature maps for graph machine learning on a neutral atom quantum processor, Phys. Rev. A **107**, 042615 (2023).

[53] M. Kornjača, H.-Y. Hu, C. Zhao, J. Wurtz, P. Weinberg, M. Hamdan, A. Zhdanov, S. H. Cantu, H. Zhou, R. A. Bravo, *et al.*, Large-scale quantum reservoir learning with an analog quantum computer, arXiv preprint arXiv:2407.02553 (2024).

[54] L. Leclerc, L. Ortiz-Gutiérrez, S. Grijalva, B. Albrecht, J. R. K. Cline, V. E. Elfving, A. Signoles, L. Henriet, G. Del Bimbo, U. A. Sheikh, M. Shah, L. Andrea, F. Ishtiaq, A. Duarte, S. Mugel, I. Cáceres, M. Kurek, R. Orús, A. Seddik, O. Hammami, H. Isselnane, and D. M'tamon, Financial risk management on a neutral atom quantum processor, Phys. Rev. Res. **5**, 043117 (2023).

[55] K. Li, J.-H. Wang, Y.-B. Yang, and Y. Xu, Symmetry-protected topological phases in a Rydberg glass, Phys. Rev. Lett. **127**, 263004 (2021).
[56] Z. Yue, Y.-F. Mao, X. Liang, Z.-X. Hua, P. Ge, Y.-X. Chao, K. Li, C. Jia, M. K. Tey, Y. Xu, and L. You, Observing structural disorder induced interacting topological phase in an atom array, arXiv:2505.06286 https://doi.org/10.48550/arXiv.2505.06286 (2025).
[57] S. Julià-Farré, J. Vovrosh, and A. Dauphin, Amorphous quantum magnets in a two-dimensional Rydberg atom array, Phys. Rev. A **110**, 012602 (2024).
[58] H. Yeo, H. E. Kim, and K. Jeong, Approximating maximum independent set on Rydberg atom arrays using local detunings, Adv. Quantum Technol. **8**, 2400291 (2025).
[59] K. Goswami, R. Mukherjee, H. Ott, and P. Schmelcher, Solving optimization problems with local light-shift encoding on Rydberg quantum annealers, Phys. Rev. Res. **6**, 023031 (2024).
[60] G. Bornet, G. Emperauger, C. Chen, F. Machado, S. Chern, L. Leclerc, B. Gély, Y. T. Chew, D. Barredo, T. Lahaye, N. Y. Yao, and A. Browaeys, Enhancing a many-body dipolar Rydberg tweezer array with arbitrary local controls, Phys. Rev. Lett. **132**, 263601 (2024).
[61] M. Kornjača, H.-Y. Hu, C. Zhao, J. Wurtz, P. Weinberg, M. Hamdan, A. Zhdanov, S. H. Cantu, H. Zhou, R. A. Bravo, K. Bagnall, J. I. Basham, J. Campo, A. Choukri, R. DeAngelo, P. Frederick, D. Haines, J. Hammett, N. Hsu, M.-G. Hu, F. Huber, P. N. Jepsen, N. Jia, T. Karolyshyn, M. Kwon, J. Long, J. Lopatin, A. Lukin, T. Macrì, O. Marković, L. A. Martínez-Martínez, X. Meng, E. Ostroumov, D. Paquette, J. Robinson, P. S. Rodriguez, A. Singh, N. Sinha, H. Thoreen, N. Wan, D. Waxman-Lenz, T. Wong, K.-H. Wu, P. L. S. Lopes, Y. Boger, N. Gemelke, T. Kitagawa, A. Keesling, X. Gao, A. Bylinskii, S. F. Yelin, F. Liu, and S.-T. Wang, Large-scale quantum reservoir learning with an analog quantum computer (2024), arXiv:2407.02553 [quant-ph].
[62] A. Radnaev, W. Chung, D. Cole, D. Mason, T. Ballance, M. Bedalov, D. Belknap, M. Berman, M. Blakely, I. Bloomfield, *et al.*, Universal neutral-atom quantum computer with individual optical addressing and non-destructive readout, PRX Quantum **6**, 030334 (2025).
[63] See supplemental material. (2025).
[64] L. Brodoloni, J. Vovrosh, S. Julià-Farré, A. Dauphin, and S. Pilati, Amorphous arrays used in "Spin-glass quantum phase transition in amorphous arrays of Rydberg atoms", 10.5281/zenodo.15276169 (2025).
[65] F. Becca and S. Sorella, *Quantum Monte Carlo approaches for correlated systems* (Cambridge University Press, 2017).
[66] E. M. Inack, G. E. Santoro, L. Dell'Anna, and S. Pilati, Projective quantum Monte Carlo simulations guided by unrestricted neural network states, Phys. Rev. B **98**, 235145 (2018).
[67] S. Pilati and P. Pieri, Simulating disordered quantum Ising chains via dense and sparse restricted Boltzmann machines, Phys. Rev. E **101**, 063308 (2020).
[68] E. M. Inack, G. Giudici, T. Parolini, G. Santoro, and S. Pilati, Understanding quantum tunneling using diffusion Monte Carlo simulations, Phys. Rev. A **97**, 032307 (2018).
[69] K. Ghanem, N. Liebermann, and A. Alavi, Population control bias and importance sampling in full configuration interaction quantum Monte Carlo, Phys. Rev. B **103**, 155135 (2021).
[70] J. Brand, M. Yang, and E. Pahl, Stochastic differential equation approach to understanding the population control bias in full configuration interaction quantum Monte Carlo, Phys. Rev. B **105**, 235144 (2022).
[71] J. Casulleras and J. Boronat, Unbiased estimators in quantum Monte Carlo methods: Application to liquid ^{4}He, Phys. Rev. B **52**, 3654 (1995).
[72] G. Carleo and M. Troyer, Solving the quantum many-body problem with artificial neural networks, Science **355**, 602 (2017).
[73] S. Pilati, E. M. Inack, and P. Pieri, Self-learning projective quantum Monte Carlo simulations guided by restricted Boltzmann machines, Phys. Rev. E **100**, 043301 (2019).
[74] M. Bernaschi, I. González-Adalid Pemartín, V. Martín-Mayor, and G. Parisi, The quantum transition of the two-dimensional Ising spin glass, Nature 10.1038/s41586-024-07647-y (2024).
[75] M. Bernaschi, I. González-Adalid Pemartín, V. Martín-Mayor, and G. Parisi, The qisg suite: High-performance codes for studying quantum Ising spin glasses, Comput. Phys. Commun. **298**, 109101 (2024).
[76] A. D. King, J. Raymond, T. Lanting, R. Harris, A. Zucca, F. Altomare, A. J. Berkley, K. Boothby, S. Ejtemaee, C. Enderud, *et al.*, Quantum critical dynamics in a 5,000-qubit programmable spin glass, Nature **617**, 61 (2023).
[77] G. M. Crosswhite, A. C. Doherty, and G. Vidal, Applying matrix product operators to model systems with long-range interactions, Phys. Rev. B **78**, 035116 (2008).
[78] C. Krämer, J. A. Koziol, A. Langheld, M. Hörmann, and K. P. Schmidt, Quantum-critical properties of the one- and two-dimensional random transverse-field Ising model from large-scale quantum Monte Carlo simulations, SciPost Phys. **17**, 061 (2024).
[79] S. Li, H. Shao, and A. W. Sandvik, Ground state of the $s = 1/2$ Heisenberg spin chain with random ferromagnetic and antiferromagnetic couplings, Phys. Rev. Lett. **134**, 086501 (2025).
[80] O. Melchert, autoScale.py - A program for automatic finite-size scaling analyses: A user's guide, arXiv:0910.5403 https://doi.org/10.48550/arXiv.0910.5403 (2009).
[81] R. Moessner, S. L. Sondhi, and P. Chandra, Two-dimensional periodic frustrated Ising models in a transverse field, Phys. Rev. Lett. **84**, 4457 (2000).
[82] P. Narasimhan, S. Humeniuk, A. Roy, and V. Drouin-Touchette, Simulating the transverse-field Ising model on the kagome lattice using a programmable quantum annealer, Phys. Rev. B **110**, 054432 (2024).
[83] A. Young, Numerical simulations of spin glasses: Methods and some recent results, in *Computer Simulations in Condensed Matter Systems: From Materials to Chemical Biology Volume 2*, edited by M. Ferrario, G. Ciccotti, and K. Binder (Springer Berlin Heidelberg, Berlin, Heidelberg, 2006) pp. 31–44.
[84] L. Brodoloni and S. Pilati, Zero-temperature Monte Carlo simulations of two-dimensional quantum spin glasses guided by neural network states, Phys. Rev. E **110**, 065305 (2024).

[85] A. Sorge, pyfssa 0.7.6., Zenodo (2025).

[86] J. Houdayer and A. K. Hartmann, Low-temperature behavior of two-dimensional Gaussian Ising spin glasses, Phys. Rev. B **70**, 014418 (2004).

[87] J. T. Chayes, L. Chayes, D. S. Fisher, and T. Spencer, Finite-size scaling and correlation lengths for disordered systems, Phys. Rev. Lett. **57**, 2999 (1986).

[88] E. Marinari, G. Parisi, F. Ricci-Tersenghi, J. J. Ruiz-Lorenzo, and F. Zuliani, Replica symmetry breaking in short-range spin glasses: Theoretical foundations and numerical evidences, J. Stat. Phys. **98**, 973 (2000).

[89] M. A. Moore, Droplet-scaling versus replica symmetry breaking debate in spin glasses revisited, Phys. Rev. E **103**, 062111 (2021).

[90] M. A. Moore, H. Bokil, and B. Drossel, Evidence for the droplet picture of spin glasses, Phys. Rev. Lett. **81**, 4252 (1998).

[91] H. Bokil, B. Drossel, and M. A. Moore, Influence of critical behavior on the spin-glass phase, Phys. Rev. B **62**, 946 (2000).

[92] H. G. Katzgraber, M. Palassini, and A. P. Young, Monte Carlo simulations of spin glasses at low temperatures, Phys. Rev. B **63**, 184422 (2001).

[93] M. Tikhanovskaya, S. Sachdev, and R. Samajdar, Equilibrium dynamics of infinite-range quantum spin glasses in a field, PRX Quantum **5**, 020313 (2024).

[94] L. Leuzzi, G. Parisi, F. Ricci-Tersenghi, and J. J. Ruiz-Lorenzo, Dilute one-dimensional spin glasses with power law decaying interactions, Phys. Rev. Lett. **101**, 107203 (2008).

[95] H. G. Katzgraber and A. P. Young, Monte Carlo studies of the one-dimensional ising spin glass with power-law interactions, Phys. Rev. B **67**, 134410 (2003).

[96] H. D. Berry and P. Singh, Monte Carlo simulation of 2D Ising spin glass with power law decaying interactions, J. Supercond. Nov. Magn. **26**, 991 (2013).

[97] J. M. Hickey, S. Genway, and J. P. Garrahan, Signatures of many-body localisation in a system without disorder and the relation to a glass transition, J. Stat. Mech. Theory Exp. **2016**, 054047 (2016).

[98] C. L. Baldwin, C. R. Laumann, A. Pal, and A. Scardicchio, Clustering of nonergodic eigenstates in quantum spin glasses, Phys. Rev. Lett. **118**, 127201 (2017).

[99] S. Mukherjee, S. Nag, and A. Garg, Many-body localization-delocalization transition in the quantum Sherrington-Kirkpatrick model, Phys. Rev. B **97**, 144202 (2018).

[100] X. Dong, X.-L. Qi, and M. Walter, Holographic entanglement negativity and replica symmetry breaking, J. High Energy Phys. **2021** (6), 1.

[101] S.-K. Jian and B. Swingle, Phase transition in von neumann entropy from replica symmetry breaking, J. High Energy Phys. **2023** (11), 1.

[102] B. P. Marsh, R. M. Kroeze, S. Ganguli, S. Gopalakrishnan, J. Keeling, and B. L. Lev, Entanglement and replica symmetry breaking in a driven-dissipative quantum spin glass, Phys. Rev. X **14**, 011026 (2024).

[103] J. Smith, A. Lee, P. Richerme, B. Neyenhuis, P. W. Hess, P. Hauke, M. Heyl, D. A. Huse, and C. Monroe, Many-body localization in a quantum simulator with programmable random disorder, Nat. Phys. **12**, 907 (2016).

[104] M. Qiao, Z. Cai, Y. Wang, B. Du, N. Jin, W. Chen, P. Wang, C. Luan, E. Gao, X. Sun, *et al.*, Tunable quantum simulation of spin models with a two-dimensional ion crystal, Nat. Phys. **20**, 623 (2024).

[105] H. J. Manetsch, G. Nomura, E. Bataille, K. H. Leung, X. Lv, and M. Endres, A tweezer array with 6100 highly coherent atomic qubits, arXiv:2403.12021 https://doi.org/10.48550/arXiv.2403.12021 (2024).

[106] G. Pichard, D. Lim, E. Bloch, J. Vaneecloo, L. Bourachot, G.-J. Both, G. Mériaux, S. Dutartre, R. Hostein, J. Paris, B. Ximenez, A. Signoles, A. Browaeys, T. Lahaye, and D. Dreon, Rearrangement of individual atoms in a 2000-site optical-tweezer array at cryogenic temperatures, Phys. Rev. Appl. **22**, 024073 (2024).

[107] F. Liu and L.-M. Duan, Computational characteristics of the random-field Ising model with long-range interaction, Phys. Rev. A **108**, 012415 (2023).